Biomedical Signal Processing and Control 68 (2021) 102610

Contents lists available at ScienceDirect

Biomedical Signal Processing and Control

journal homepage: www.elsevier.com/locate/bspc

Analysis and classification of heart rate using CatBoost feature ranking model

B. Dhananjay , J. Sivaraman *

Bio-signals and Medical Instrumentation Laboratory, Department of Biotechnology and Medical Engineering, National Institute of Technology, Rourkela, Odisha, 769008, India

ARTICLE INFO

Keywords:
Attribute order
CatBoost model
Extra Trees model
Prediction Value Change
Ridge model

ABSTRACT

Background: In specific contexts, it is difficult to manually differentiate Sinus Rhythm (SR), Sinus Tachycardia (ST), and Atrial Tachycardia (AT) from ECG signals. Upright P-wave is a context in which it is hard to distinguish SR, ST, and AT.
Objective: The main objective of this work is to develop a machine learning model to classify SR, ST, and AT conditions from ECG. A highly-effective feature-ranking algorithm is proposed to reduce the complexity of the classification task.
Methodology: A CatBoost (CB) model is used for feature ranking. The model is synthesized using the Prediction Value Change (PVC) algorithm. The ECG features, namely P-wave (ms), PRI (ms), QRS (ms), T-wave (ms), QTI (ms), P-wave (μV), R-wave (μV), and T-wave (μV), are used as the input features of the machine learning model.
Results: The accuracy, sensitivity, precision, and F1 score of the CB machine learning model are 99 %, 99.17 %, 99.25 %, and 99 %, respectively. The computational time of the CB model is 0.0078 s. The Extra Trees (ET) and Ridge Classifier (RC) models were also developed, and their performances were compared with the CB model.
Conclusion: The accuracy, sensitivity, precision, and F1 score of the CB model perform better than ET and RC models. The CB-based machine learning model's computational time is minimal as it uses the symmetric tree-based inference system. The boosting algorithm present in the CB classifier minimizes over-fitting issues.

1. Introduction

Sinus Tachycardia (ST) is a type of heart condition where the heart rate of an adult human being beats more than 100 bpm with an effect of physical training, provided the adult human being was showing an average heart rate (60 bpm – 90 bpm) before undergoing a physical activity [1]. Atrial Tachycardia (AT) is a type of supraventricular tachycardia, and the reason for its occurrence is due to multiple mechanisms. The disorder in the heart rhythm leading to AT is the abnormal beating of atrial foci [2], triggered rhythm [3], or there is atrial re-entry [4,5]. There is no defined procedure to be followed for the treatment of different types of ST to date. Medical examiners have discretion for opting for either of the methods depending on the severity of the heart condition. The success rates of either of the plans have varied significantly in the past, thus developing complications like permanent pacing requirement [1,6–8], phrenic nerve paralysis [9], and others [10,11]. It is challenging to diagnose a tachycardia originating from a small area present in the heart's atrial part; Focal Atrial Tachycardia (FAT) is commonly called AT. The Radio-Frequency Ablation (RFA) method helps treat AT, a rare type of supraventricular tachycardia [12,13]. To overcome the challenges faced in detecting heart diseases like ST and AT manually, machine learning models are used to classify, predict, and detect various heart diseases. Kumari et al. [14] developed a Support Vector Machine (SVM) model to automatically detect Arial flutter, Ventricular flutter, Atrial, and Ventricular Fibrillation. Yildirim et al. [15] developed a deep Convolutional Neural Network (CNN) to detect different arrhythmia classes present in the ECG signal while taking 10 s ECG signal fragments as the input. Tabassum et al. [16], in their work, developed an SVM model to predict ECG signals and clinical ECG features like Heart rate (bpm), PR interval (sec), and QRS complex (sec) as the input features to the SVM model.

Many previous works [1–13,37,45] have been done on classifying Inappropriate Sinus Tachycardia (IST) with other Supra-Ventricular Tachycardia (SVT) or Atrial Tachycardia (AT) by manually inducing drugs or by clinically analysing the ECG signal. The focus on classifying Sinus Tachycardia (ST) with other SVT or AT-related arrhythmias is

* Corresponding author.
E-mail address: jsiva@nitrkl.ac.in (J. Sivaraman).

https://doi.org/10.1016/j.bspc.2021.102610
Received 31 December 2020; Received in revised form 26 February 2021; Accepted 30 March 2021
Available online 5 April 2021

rare. The previous studies [14–16] have concluded that SVM and CNN models are widely used to classify, predict, and detect various cardiac arrhythmias using ECG signals as the input. The SVM model's drawbacks are that it is not suitable for large data sets; the SVM model fails to perform well when the target classes overlap. The SVM model underperforms if the dataset is having more features than the training data samples. The SVM classifier classifies data based on a hyperplane, resulting in no proper explanation for the data classification. The CNN model's major disadvantage is that it takes more time in computing and is prone to overfitting. The work's novelty lies in proposing a Prediction Value Change (PVC) algorithm to clinically rank the ECG features and develop a CatBoost model to classify SR, ST, and AT based on the PVC algorithm.

The main problem being addressed in this work is to analyse and classify SR, ST, and AT using the basic ECG features (Heart rate (bpm), PPI (ms), P-wave (ms), PRI (ms), QRS (ms), T-wave (ms), QTI (ms), P-wave (μV), R-wave (μV), T-wave (μV)). The rationale for doing this work is, as it is a cumbersome process to differentiate SR, ST, and AT ECG signals manually. In this work, SR, ST, and AT ECG signal classification was done using a new proposed PVC algorithm by developing a CatBoost machine learning model. The CatBoost machine learning model's use does not give more importance to the less significant features. The proposed PVC algorithm has a training phase and testing phase. In this work, only one public database was used of the Chapman University and Shaoxing People's Hospital (CUSPH) to obtain 10 s AT ECG signal, and for SR and ST group, the ECG signals were recorded for 60 s using EDAN SE 1010 PC ECG instrument. A self-made dataset was created using 10 s ECG signal of the SR and ST group and combined with 10 s ECG signal of AT patients from the CUSPH database. The basic ECG features were manually extracted from SR, ST, and AT ECG signals. The machine learning models' input data consisted of 150 data points with 11 features for the training stage: 70 % of the data was used, and for the testing stage: 30 % of the data. In this work, the developed machine learning models are Extra Trees (ET), Ridge Classifier (RC), and CatBoost (CB). The CB-based machine learning model is the primary focus of this work. The advantages of the CB-based machine learning model are that computational time is minimal, the inference drawn is very fast as it uses the symmetric trees approach, and the boosting algorithm present in the CB classifier minimizes overfitting of the model. The method proposed in this work differs from previous works done as CB based classifier has not been used to classify ECG data of different heart rates.

2. Methodology

2.1. Data acquisition

The ECG recordings were recorded inside the National Institute of Technology Rourkela premises, and the volunteers were students of the institute. In this study, sinus rhythm was the only inclusion criteria, and no other specific criteria were used in the study. In this study, the exclusion criteria were volunteers having severe medical conditions or taking medication for the past six months resulting in altering the ECG parameters, smokers and alcoholics, hypertensive, heart rhythm problems, congenital heart defects, and heart valve disease patients [17,38,40]. A total of 50 male volunteers with a mean age of 25 ± 5 years participated in the study. The ECG recorded using the EDAN SE 1010 PC ECG instrument, and the recording carried out using the standard 12-lead ECG recording system. The sampling frequency of the instrument was 1000 Hz. The ECG signal recording for SR and ST stages followed a standard paper speed with 25 mm/s and 10 mm/mV for 60 s each in the supine position. The volunteers underwent skin preparation, which involved shaving and cleaning with isopropyl alcohol before recording. The ECG recording happened in two phases.

The first phase was called the SR stage, where the ECG was recorded in the supine position, and the second phase was called the ST phase, where the volunteers performed a physical task before recording the ECG. Physical activity is divided into isometric, isotonic, and resistance [18,19]. In this study, the resistance type of exercise method was used. The volunteers were made to run for 100 m, and then they lifted a 5 kg weight bag. The AT ECG signals were obtained from Chapman University and Shaoxing People's Hospital (CUSPH) database [20] of 50 patients with a mean age of 50 ± 12 years and a sampling frequency of 500 Hz. The length of the ECG recording in every case was 10 s, and Lead II was preferred. R-peaks were detected using the amplitude threshold technique. Clinical ECG features were manually analyzed for feature extraction [21–25]. Machine learning models based on ET, RC, and CB were used for feature ranking and classification of SR, ST, and AT, as shown in Fig. 1.

2.2. Pre-processing

The filters present in the recording instrument were baseline drift filter (strong), low pass filter (75 Hz), and AC filter (50 Hz) was employed to remove the noise present in the recorded ECG signal. The AT ECG signals were taken from Chapman University and Shaoxing People's Hospital (CUSPH) database, which provides a de-noised ECG signal.

2.3. Feature extraction

The recorded ECG signal can be viewed with a magnifying factor of 200 mm/s and 100 mm/mV, which assists in the manual extraction of the features. The clinical features extracted from the ECG signals were PPI (ms), P-wave (ms), PRI (ms), QRS (ms), T-wave (ms), QTI (ms), P-wave (μV), R-wave (μV), and T-wave (μV). These clinical features give first-hand information of any abnormality observed in the ECG signal. The error in manual and machine reading showed ±2 ms and ±0.02 μV, which seems negligible as an effect of inter and intraobserver variability. The P-wave morphology was the essential clinical feature for manually analysing SR, ST, and AT ECG signals. If the P-wave is inverted and the voltage is between -15μV to -25μV, it is diagnosed as AT by analysing other clinical ECG features. If the P-wave deflected upright, then it becomes difficult to distinguish between SR, ST, and AT manually. Thus, the selected features play an important role in classifying SR, ST, and AT ECG signals.

$$PPI = (P_{on+1} - P_{on}) \tag{1}$$

$$\mathrm{P}_{dur} = P_{off} - P_{on} \tag{2}$$

$$PRI = Q_{on} - P_{on} \tag{3}$$

$$P_{amp} = \max(x[i])i \in [P_{on}\, P_{off}] \tag{4}$$

2.4. Feature evaluation

In this work, the significance of the data assorted in the self-made dataset underwent the *t*-test with two-tailed distribution and two-sample unequal variance (heteroscedastic) test. The values of the features incorporated in the dataset showed a P-value <0.05. The SR ECG signal values were taken as a base to calculate the P-values, i.e., SR vs. ST ($P < 0.05$) and SR vs. AT ($P < 0.05$), as shown in Table 1. The features were evaluated based on the developed machine learning models. The classifiers selected for feature evaluation were:

2.4.1. ET classifier

ET classifier, also called Extremely Randomized Tree Classifier, is based on the principle of bagging. In these methods, the built ensemble model improves prediction accuracy by decreasing the model's variance. It reduces by combining the predictions of the individual models used for training and the training samples generated. The final prediction of the developed ensemble model is made by averaging each

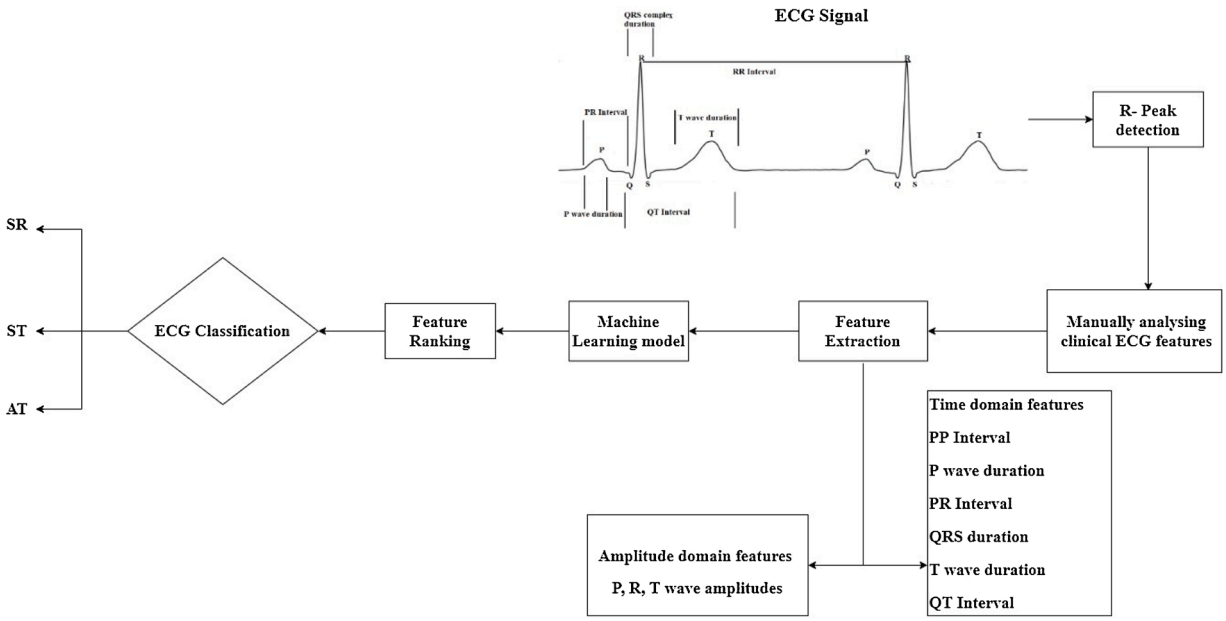

Fig. 1. Block diagram of the proposed work.

Table 1
Statistical analysis of the self-made dataset.

Features	SR (Mean ± SD)	ST (Mean ± SD)	AT (Mean ± SD)	P-value* (SR vs. ST), (SR vs. AT)
Age (years)	25 ± 5	25 ± 5	50 ± 12	–
Heart rate (bpm)	74 ± 6.60	105 ± 3.93	93 ± 14.04	<0.05
PPI (ms)	832 ± 70.81	568 ± 19.84	660 ± 125.18	<0.05
P-wave (ms)	96 ± 9.86	75 ± 6.60	68 ± 11.63	<0.05
PRI (ms)	137 ± 21.77	97 ± 10.15	152 ± 19.61	<0.05
QRS (ms)	86 ± 5.73	79 ± 5.93	80 ± 9.84	<0.05
T-wave (ms)	176 ± 33.01	144 ± 32.32	149 ± 25.47	<0.05
QTI (ms)	332 ± 37.16	256 ± 25.49	345 ± 17.32	<0.05
P-wave (μV)	105 ± 19.26	138 ± 14.58	−32 ± 42.69	<0.05
R-wave (μV)	1245 ± 141.20	1300 ± 135.07	1020 ± 164.27	<0.05
T-wave (μV)	292 ± 123.30	238 ± 121.09	206 ± 121.45	<0.05

* UnpairedStudent's *T*-Test.

estimator's predictions. The ET classifier is a combination of the decision trees classifier and random forest classifier. The developed algorithm in the ET classifier works on entropy and information gain.

$$E = \sum_{i=1}^{c} -p_i log_2 p_i \tag{5}$$

E represents entropy, c represents the number of classes present in the given dataset, and p_i represents the number of rows for each type denoted in the dataset.

$$\gamma(S,A) = E(S) - \sum_{v\epsilon(A)} \frac{S_v}{S} E(S_v) \tag{6}$$

γ represents Information Gain, E represents entropy, S is the probability of the condition's occurrence, and A represents the attribute or feature taken into consideration, v means the individual values present in that particular feature or characteristic, S_v represents the probability of that particular individual value to occur.

2.4.2. RC classifier

The RC classifier works on the principle of L2 regularization. L2 regularization means considering the sum of squares of coefficient while optimizing the function. Eq. (7). represents the optimization process of the Ridge classifier

$$O = \lambda + \acute{E}\, c^2 \tag{7}$$

O represents the optimization process, λ represents the error, É represents the emphasis, and c^2 represents the coefficients' square.

$$Y = \lambda + \alpha(w^2) \tag{8}$$

Substituting output as Y, input as x, weights as w, error as λ, and α as the weights' coefficient then Eq. (8). becomes

$$Y = \sum_{i=1}^{N} \left\{ y_i - \sum_{j=0}^{M} w_j x_{ij} \right\}^2 + \alpha \sum_{j=0}^{M} w_j^2 \tag{9}$$

Eq. (9). represents Eq. (8). after substituting the variables

$$\frac{\partial}{\partial w_j}(Y) = -2 \sum_{i=1}^{N} x_{ij} \left\{ y_i - \sum_{k=0}^{M} w_k x_{ik} \right\} + 2\alpha w_j \tag{10}$$

Eq. (10). is the derivative of Eq. (9). resulting in calculating the Gradient of the Ridge classifier.

$$w_j^{t+1} = (1 - 2\alpha\eta) w_j^t + 2\eta \sum_{i=1}^{N} x_{ij} \left\{ y_i - \sum_{k=0}^{M} w_k x_{ik} \right\} \tag{11}$$

The Gradient of the Ridge Classifier is shown in Eq. (10). is after applying the regularization (L2) method shown in Eq. (11). After using the Gradient regularization method, the weight factor w_j remains, and the rest of all the weight factors result in zero. All these weights get updated by the regularization part, and $1 - 2\alpha\eta$ is the weight-reducing factor.

2.4.3. CB classifier

CatBoost machine learning algorithm is a particular type of Gradient boosting on the decision trees as it can handle categorical, ordered features, and the overfitting of the model is taken care of by Bayesian

estimators. The CatBoost machine-learning algorithm uses Prediction Values Change (PVC) or Loss Function Change (LFC) to rank the developed model's features. PVC works on calculating the change in prediction observed when a value corresponding to the feature changes. PVC is a default method used in CatBoost based machine learning models. LFC is generally used to rank a particular model among a range of models. PVC is one of the feature ranking-based methods embedded in the developed CatBoost machine learning model in this work.

$$F = \{f_1, f_2, f_3, \ldots\ldots\ldots f_n\} \tag{12}$$

$$P_i = \beta_i F_j \tag{13}$$

F represents a set of input features, β as the numeric factor assigned to the input features, P as predicting that particular step. Eq. (12). represents the feature set given to the machine learning model. In Eq. (13). P_i represents the prediction value at a substituted numeric factor, β_i represents the numeric factor, and F_j represents the particular feature selected from the given feature set.

$$P_{i+1} = \beta_{i+1} F_j \tag{14}$$

$$P_{i=0} \neq P_i \neq P_{i+1} \tag{15}$$

Eq. (14). P_{i+1} states the prediction value when the numeric factor is changed, β_{i+1} states the modified numeric factor. Eq. (15). says that when there is a change in the numeric factor and changes the prediction value, that particular feature is necessary

2.5. Testing and training dataset

The dataset created based on the clinical features of the ECG signal like Heart rate (bpm), PPI (ms), P-wave (ms), PRI (ms), QRS (ms), T-wave (ms), QTI (ms), P-wave (μV), R-wave (μV), and T-wave (μV). The dataset consisted of three classes: SR, ST, and AT, and manually assigned each target value. The value of SR, ST, and AT in the Target variable is represented by 0, 1, and 2, respectively. All three classifiers were developed and compared in this work. The ratio of 0.7 to 0.3 was considered for training and testing, respectively. The shape of the original dataset, i.e., the self-made dataset, was in 150 rows to 11 columns, and there was no missing data in the self-made dataset. The features encoded in the self-made dataset and into the machine learning model displayed numeric values. There were no categorical features encoded in the self-made dataset. There were no ordinal, and neither were there high cardinal features present in the self-made dataset. The valid sampled noticed in the dataset were 142 with eleven elements, including the Target variable. The samples considered for the training and testing set were 99 and 43, respectively, and all the data classes had equal weightage. The selection of training and testing data set was random as manual selection makes the model more error-prone and time-consuming [26]. The training and testing dataset were shuffled to validate the extracted features because the machine learning algorithms depend on the input features and also to check the robustness of the considered machine learning classifiers [27–29].

2.6. Hardware and software requirements

This work's only hardware requirement is to record the ECG signals using EDAN SE 1010 PC ECG instrument. The ECG instrument performed the pre-processing of the ECG signals of SR and ST. The AT ECG signals provided in the CUSPH database were noise-free. The developments of the machine learning models, training, and testing were performed in Google colab.

2.7. Performance analysis

The developed ET and RC machine learning models were compared with the proposed CB model. The comparison was made based on commonly used performance analysis metrics. The performance analysis metrics consisted of Accuracy, Sensitivity, Precision, F1 score, and computational time. The formulas used to calculate the performance analysis for all the machine learning models given below:

$$Accuracy = \frac{True\ Positive + True\ Negative}{Total\ Samples} \tag{16}$$

$$Sensitivity = \frac{True\ Positives}{True\ Positives + False\ Negatives} \tag{17}$$

$$Precision = \frac{True\ Positives}{True\ Positives + False\ Positives} \tag{18}$$

$$F1\ score = 2\left(\frac{1}{\frac{1}{Precision} + \frac{1}{Sensitivity}}\right) \tag{19}$$

3. Results

3.1. Statistical analysis

The boxplot displayed in Fig. 2a divulges PPI (ms) information for SR, ST volunteers, and AT patients. The boxplot's x-axis represents the data classes, and the y-axis displays the PPI (ms). The minimum PPI (ms) for SR and ST volunteers and AT patients was 674 (ms), 531 (ms), and 513 (ms), respectively. The maximum PPI (ms) for SR and ST volunteers and AT patients was 974 (ms), 605 (ms), and 800 (ms), respectively. Fig. 2b exhibits the P-wave (ms) of SR, ST volunteers, and AT patients. The boxplot's x-axis represents the different classes present in the data, and the y-axis represents the P-wave (ms). The minimum P-wave (ms) of SR volunteers was 80 (ms). The minimum P-wave (ms) for ST volunteers was 62 (ms). The minimum P-wave (ms) of AT patients was 48 (ms). The maximum P-wave (ms) of SR volunteers is 118 (ms), for ST volunteers is 88 (ms), and for AT patients, it is 100 (ms). Fig. 2c demonstrates PRI's (ms) boxplot for SR, ST volunteers, and AT patients. The boxplot's x-axis represents the class of the data present, and the y-axis shows the PRI (ms). The minimum PRI (ms) for SR, ST volunteers, and AT patients was 100 (ms), 76 (ms), and 121 (ms), respectively. The maximum PRI (ms) for SR, ST volunteers, and AT patients was 182 (ms), 115 (ms), and 194 (ms), respectively. Fig. 3a exhibits the P-wave (μV) of SR and ST volunteers and AT patients. The boxplot's x-axis represents the different classes present in the data, and the y-axis represents the absolute P-wave (μV). The minimum absolute P-wave (μV) of SR volunteers was 75 (μV). The minimum absolute P-wave (μV) for ST volunteers was 105 (μV). The minimum absolute P-wave (μV) of AT patients was 15 (μV). The maximum absolute P-wave (μV) of SR volunteers is 151 (μV), for ST volunteers, it is 172 (μV), and for AT patients, it is 117 (μV). Fig. 3b reveals the R-wave (μV) boxplot for SR, ST volunteers, and AT patients. The x-axis denotes the number of data present, and the y-axis indicates the R-wave (μV). The minimum R-wave (μV) for SR, ST volunteers, and AT patients were 997 (μV), 1067 (μV), and 823 (μV), respectively. The maximum R-wave (μV) for SR, ST volunteers, and AT patients were 1467 (μV), 1517 (μV), and 1463 (μV), respectively. Fig. 3c divulges T-wave (μV) boxplot for SR, ST volunteers, and AT patients. The boxplot's x-axis shows the number of classes present in the data, and the y-axis shows the T-wave (μV). The minimum T-wave (μV) for SR, ST volunteers, and AT patients were 122 (μV), 72 (μV), and 46 (μV), respectively. The maximum T-wave (μV) for SR, ST volunteers, and AT patients were 480 (μV), 430 (μV), and 405 (μV), respectively.

3.2. ET based machine learning model

Fig. 4a displays the ET model's essential features. According to the developed model, P-wave (μV), PPI (ms), and P-wave (ms) are the essential features to classify SR, ST, and AT ECG signals. The x-axis of the

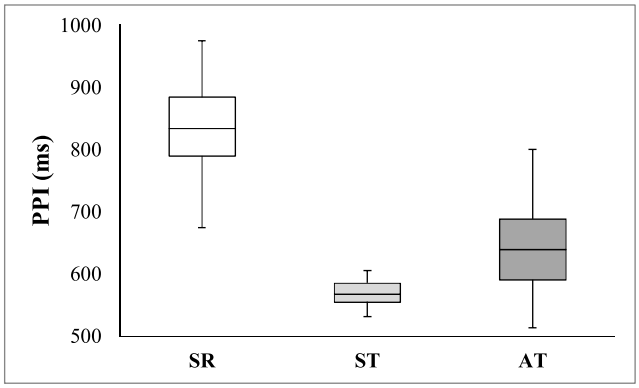

a

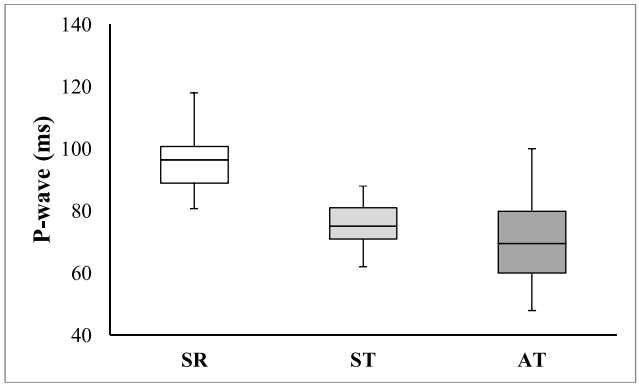

b

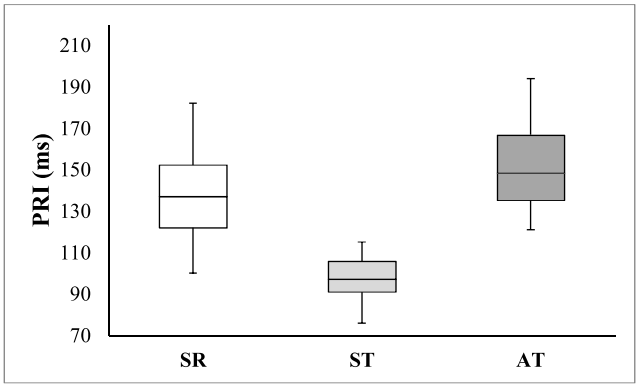

c

Fig. 2. a Boxplot of PP interval for SR, ST volunteers and AT patients.
b Boxplot of P-wave duration of SR, ST volunteers and AT patients.
c Boxplot of PR interval for SR, ST volunteers, and AT patients.

graph denotes the variable importance, and the y-axis represents the features. The features P-wave (μV) showed variable importance of 0.30, PPI (ms) displayed 0.26. The P-wave (ms) characteristic was ranked third by the ET model with a variable volume of 0.20. The model ranked the features PRI (ms), T-wave (μV), and QRS (ms) as the last three essential features. According to the developed ET model, the crucial element was P-wave (μV), and the least essential characteristic was the QRS (ms).

3.3. RC based machine learning model

Fig. 4b displays the essential features ranked by the RC model. According to the developed model, PRI (ms), QTI (ms), and P-wave (ms)

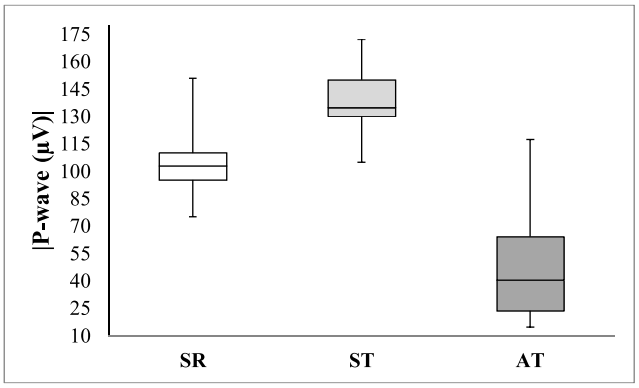

a

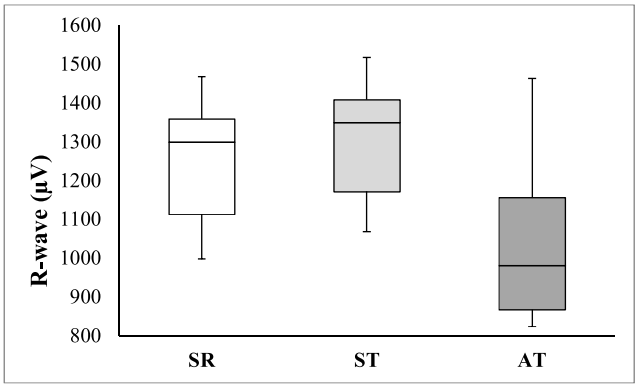

b

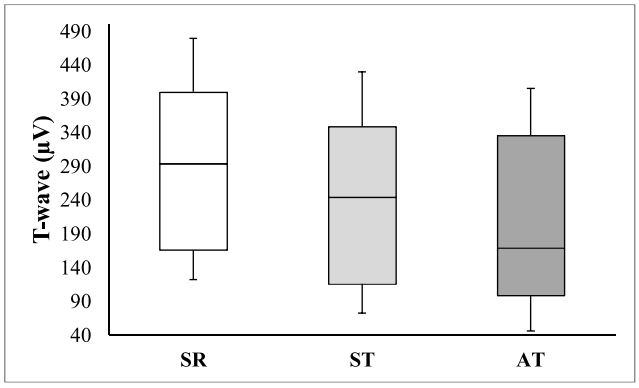

c

Fig. 3. a Boxplot of absolute P-wave amplitude of SR, ST volunteers, and AT patients.
b Boxplot of R-wave amplitude of SR, ST, and AT patients.
c Boxplot of T-wave amplitude for SR, ST volunteers, and AT patients.

are the essential features to classify SR, ST, and AT ECG signals. The x-axis of the graph denotes the variable importance, and the y-axis represents the features. The features PRI (ms) showed variable importance of 0.0085; QTI (ms) displayed 0.0075. The P-wave (ms) characteristic was ranked third by the RC model with variable importance of 0.0058. The model ranked the features QRS (ms), T-wave (μV), and R-wave (μV) as the last three essential features. According to the developed RC-based model, the most crucial element was PRI (ms), and the least essential characteristic was the R-wave (μV).

3.4. CB based machine learning model

Fig. 4c shows the essential features ranked by the developed CB-based machine learning model. The model has rated PPI (ms), P-wave

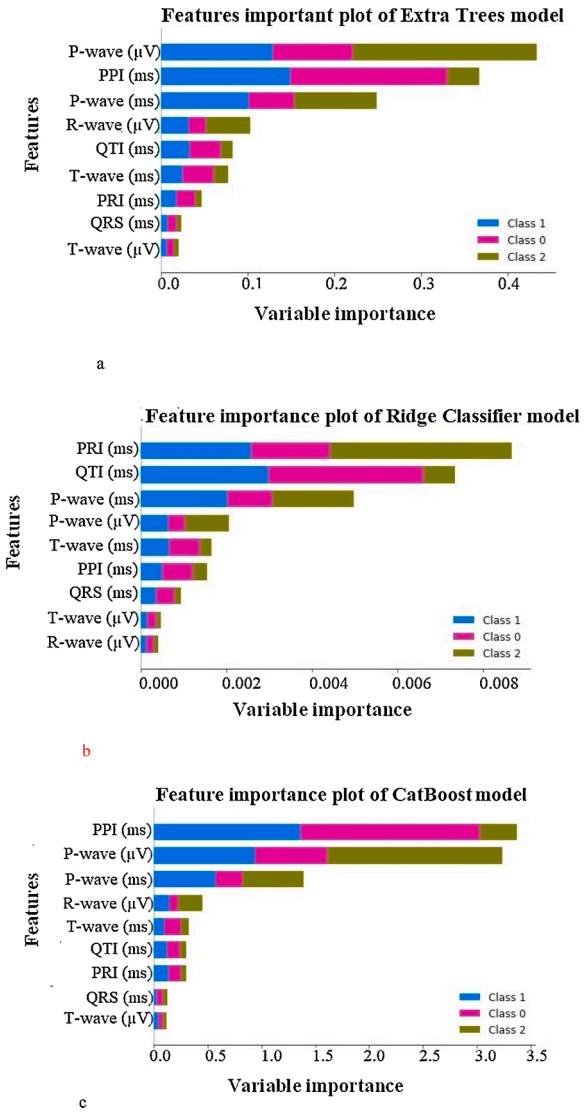

Fig. 4. a Feature importance plot generated by the Extra Trees model. b Feature importance plot generated by the Ridge Classifier model. c Feature importance plot of CatBoost based machine learning model.

(μV), and P-wave (ms) as the most crucial features for classifying SR, ST, and AT ECG signals. The least essential element for classifying SR, ST, and AT is the T-wave (μV). Table 2 shows the critical feature ranked from most important to the least important by each model. The most clinically significant features organized by the developed models to classify SR, ST, and AT are P-wave (μV), PRI (ms), and PPI (ms). The least clinically significant features ranked by the developed models to classify SR, ST, and AT ECG signals are QRS (ms), R-wave (μV), and T-wave (μV). Table 3 displays the summary of different available machine learning models used in the classification of abnormal ECG signals, and they are compared with the proposed machine learning model in terms of accuracy, sensitivity, and precision. Table 4 divulges the information of all other machine learning classifiers considered in this work.

Table 2
Summary of importance of features given by each model.

Models	Most important feature	Least important feature
ET	P-wave (μV)	QRS (ms)
RC	PRI (ms)	R-wave (μV)
CB	PPI (ms)	T-wave (μV)

4. Discussion

Manolis et al. [30] correctly identified a FAT ECG signal using atrial rate and abnormal P wave morphology and noted negative P wave. Zedda et al. [31] identified different P wave morphology in FAT patients and concluded a negative P wave in observation. Tanabe et al. [32] studied an 80-year-old woman diagnosed with paroxysmal atrial fibrillation, and on examining her with 12 lead ECG, found that an inverted P wave in inferior leads. Morris et al. [33], while studying AT from Cristae Terminalis, observed that the P wave was negative in 50 patients in lead V_1 among 78 patients. In the rest, 20 patients, the P wave followed was positive. Li et al. [34] studied AT caused by the right atrium in a 74-year-old healthy man. The study's subject was under the initiation of AT, and on examination, the P wave recorded was positive in leads I, II, III, aVF, and V1. Hayashi et al. [35] concluded that P wave morphology and intracardiac activation time are critical clinical aspects to understand FAT better. They also state that four different P wave types are observed in FAT, determining FAT's origin. Sonsoz et al. [36], in their work, studied a pregnant woman suffering from FAT. The analysis showed a heart rate at 134 bpm, and the P wave was negative in the lateral leads and positive in lead V1. Sonsoz et al. [36] depicted the observed P wave morphology is evident in AT originating from the Left atrial appendage. Eckhardt et al. [37], in their work on Inappropriate Sinus Tachycardia (IST), concluded to differentiate IST, Postural Orthostatic Tachycardia Syndrome (POTS), and FAT, a detailed analysis of P wave morphology is required.

From the previous studies [30–37], the prediction given by the models developed in this work is in line. The developed ET model predicted P wave is one of the clinical features that can classify SR, ST, and AT ECG signals. The P wave observed in AT patients was malicious; a few studies [31,33,35] have also observed the same phenomenon. Thus, the developed ET model's P wave prediction is critical for clinical features per study [38–44].

Nagashima et al. [45] studied a 75-year-old patient suffering from the chronic obstructive pulmonary disease without any structural heart disease sign. The ECG analysis of the particular patient showed a prolonged PRI and a short QRS. One previous study [45] also stated that a longer PRI indicates AT cardiac abnormality, and the studies [37,46] have observed a direct relation between PRI and Heart rate in FAT patients. Field et al. [46] observed an increase in P wave and the absence of PRI lengthening in IST volunteers. Madaffari et al. [47] concluded that the PRI could be used as a guide to confirm the atrial blocks present in the heart. A study conducted by Sivaraman et al. [48] on analysing SR and AT by developing an ARX model concluded that the atrial repolarization phase (PTaI) shows the most instability. As the PTaI is observed in a modified limb lead system (MLL) and not visible in the SLL system, the PRI masks it. Thus PRI can be used to classify SR, ST volunteers, and AT patients. Cabrera et al. [49] observed that a prolonged PRI is a clinical indication of Atrial Fibrillation's onset. Pavri et al. [50] observed an abnormal behavior of the PRI in COVID-19 patients. The statistical results and the developed machine learning model results comply with the previous studies [37,45–50] in the PRI aspect. The developed RC model predicted that the PRI is one of the clinical aspects of classifying SR, ST volunteers, and AT patients.

Banavalikar et al. [51] diagnosed FAT based on atrial rate ranging from 100 bpm to 240 bpm. Kang et al. [52] differentiated ST from FAT with the help of the atrial rate. The atrial rate observed between ST and AT differed by 150 % in their work, where the AT atrial rate was higher than the ST atrial rate. Dhananjay et al. [53] concluded that the PPI observed in ST volunteers is comparatively less than SR volunteers as the heart rate increases; the intervals' length decreases. Eckhardt et al. [37] observed that the PPI is the clinical aspect to diagnose, classify, and predict SR and IST. The results presented in this work align with the previous studies [37,51–53] in the PPI. The statistical analysis presented in this work shows that the PPI for SR volunteers is more than the ST volunteers and AT patients. In this work, the developed CB model also

Table 3
Comparison of the proposed method with previously available machine learning methods.

Study, Year	Features Selected	Classifier Used	Accuracy	Sensitivity	Precision	Number of subjects	Data Length	Database used
[54], 2016	Independent Component Analysis, Principal Component Analysis, Discrete Wavelet Transform	Support Vector Machines	98.91 %	98.9 %	98.9 %	47	30 minutes	MIT-BIH
[57], 2017	Projections, Weighted RR intervals	Support Vector Machines	98.46 %	98.46 %	95.4 %	47	30 minutes	MIT-BIH
[58], 2017	Higher-order statistics and spectra	Principal Component Analysis, K Nearest Neighbors, Decision Trees	98.17 %	94.57 %	–	40 (SR) 17 (CAD)	30 minutes 2 h	Fanatasia St. Petersburg
[15], 2018	Raw ECG signal	Convolutioal Neural Networks	95.2 %	93.52 %	92.52 %	45	10 s	MIT-BIH
[56], 2019	Local Binary Pattern, Higher Order Statistics	Support Vector Machines	94.5 %	70.3 %	66.4 %	47	30 minutes	MIT-BIH
[55], 2020	Q-wavelet transform	Support Vector machines	99.27 %	96.22 %	–	47	30 minutes	MIT-BIH
[14], 2020	Discrete Wavelet Transform	Support Vector Machines	95.92 %	92.59 %	96.11 %	162*	NA	MIT-BIH & BIDMC
Proposed method	**Clinical ECG features**	**CatBoost**	99 %	99.17 %	99.25 %	**150**	10 s	**Data collected & CUSPH**

NA-Not Available.
* The input features were more than the number of subjects. Hence the SVM model underperforms.

Table 4
Summary of all the classifiers considered.

Model	Accuracy	Sensitivity	Precision	F1	Kappa	MCC	TT(sec)
ET	0.99	0.99	0.99	0.99	0.99	0.99	0.2401
RC	0.99	0.99	0.99	0.99	0.99	0.99	1.2493
CB	0.99	0.9917	0.9925	0.99	0.9851	0.9864	0.0078
KNN	0.98	0.9778	0.9845	0.9793	0.9695	0.9721	0.2307
LDA	0.98	0.9778	0.9867	0.9770	0.9688	0.9737	0.0044
LGB	0.98	0.9806	0.9845	0.9796	0.9697	0.9723	0.0291
LR	0.96	0.9556	0.9637	0.9576	0.9377	0.9419	0.0387
DT	0.96	0.9639	0.9730	0.9589	0.9405	0.9476	0.0048
QDA	0.96	0.9583	0.9670	0.9593	0.9392	0.9429	0.0043
AB	0.95	0.9444	0.9374	0.9384	0.9218	0.9348	0.0767
RF	0.93	0.9333	0.9420	0.9293	0.8944	0.9009	0.1116
NB	0.91	0.9	0.9378	0.9003	0.8613	0.8799	0.0049
SVM	0.71	0.7250	0.7466	0.6611	0.5747	0.6269	0.10703

concluded that the atrial rate helps diagnose, classify SR, ST, and AT patients.

5. Conclusion

In this work, the time durational and amplitude characteristics of the ECG signal of SR, ST volunteers, and AT patients acted as the machine learning models' feature set. The dataset was created based on the clinical features of the ECG signal like Heart rate (bpm), PPI (ms), P wave (ms), PRI, QRS (ms), T wave (ms), QTI (ms), P wave (μV), R wave (μV), and T wave (μV). Three different machine learning models developed in this work are ET, RC, CB. The developed CB model performed better than the developed ET and RC model based on sensitivity and precision. The machine learning models based on feature importance concluded that P wave (μV), PRI (ms), and Atrial rate (PPI (ms)) could accurately classify SR, ST, and AT ECG signals. The advantages of the CB-based machine learning model are that the computational time is minimal, the inference drawn is very fast as it uses the symmetric trees approach, and the boosting algorithm imbibed in the CB classifier minimizes overfitting of the model.

6. Future scope

In this work, the authors wanted to validate the algorithm in clinical aspects. Hence the results have been more clinically determined. The algorithm's validation was carried out in two phases, the first phase being clinically ranking the importance of basic ECG features in classifying SR, ST, and AT ECG signals and the second phase being the performance metrics. The metrics for comparison were: accuracy, sensitivity, precision, F1 score, and total time (sec) to execute. There have been many studies [59–63] where the machine learning models are being implemented on a wearable device to detect various cardiac arrhythmias in real-time. In the future, the proposed CB model can be implemented in the hardware as it has performed well in the clinical aspects.

Funding

The present study was supported by financial grants from the Science Engineering Research Board (SERB), Department of Science and Technology (DST), Government of India (EEQ/2019/000148).

Ethical approval

All procedures performed in studies involving human participants were in accordance with the ethical standards of the institutional committee and with the 1964 Helsinki declaration and its later amendments or comparable ethical standards.

Informed consent

Informed consent was obtained from all individual participants included in the study.

CRediT authorship contribution statement

B. Dhananjay: Conceptualization, Methodology, Software, Validation, Formal analysis, Investigation, Resources, Writing - original draft, Writing - review & editing, Visualization. **J. Sivaraman:** Conceptualization, Methodology, Validation, Formal analysis, Resources, Data curation, Writing - review & editing, Visualization, Supervision, Project administration, Funding acquisition.

Declaration of Competing Interest

The authors report no declarations of interest.

Acknowledgments

The authors acknowledge the support from the Ministry of Education, Government of India to carry out this research work.

References

[1] S.F. Nagueh, I. Mikati, H.A. Kopelen, K.J. Middleton, M.A. Quinones, W.A. Zoghbi, Doppler estimation of left ventricular filling pressure in sinus tachycardia : a new application of tissue doppler imaging, Circulation 98 (16) (1998) 1644–1650, https://doi.org/10.1161/01.CIR.98.16.1644.

[2] P.C. Gillette, F.C. Cravord, V.L. Zeigler, Mechanisms of atrial tachycardias, in: D. P. Zipes, J. Jalife (Eds.), Cardiac Electrophysiology; From Cell to Bedside, Saunders, Philadelphia, 1990, pp. 559–563.

[3] A.L. Wit, M.R. Rosen, et al., After depolarizations and triggered activity, in: H. A. Fozzard, E. Haber, R.B. Jennings (Eds.), The Heart and Cardiovascular System, Raven Press, New York, 1986, pp. 1449–1490.

[4] D.E. Haines, J.P. DiMarco, Sustained intraatrial recntrant tachycardia: clinical electrocardiographic and electrophysiologic characteristics and long term follow-ups, J. Am. Coll. Cardiol. 15 (1990) 1345–1354, https://doi.org/10.1016/s0735-1097(10)80025-7.

[5] C.W. Tang, M.M. Scheinman, G.F. Van Hare, L.M. Epstein, Use of P wave configuration during atrial tachycardia to predict site of origin, J. Am. Coll. Cardiol. 26 (5) (2000) 1315–1324, https://doi.org/10.1016/0735-1097(95)00307-X.

[6] A.D. Krahn, R. Yee, G.J. Klein, C. Morillo, Inappropriate sinus tachycardia: evaluation and therapy, J. Cardiovasc. Electrophysiol. 6 (12) (1995) 1124–1128, https://doi.org/10.1111/j.1540-8167.1995.tb00391.x.

[7] B. Olshansky, What's so inappropriate about sinus tachycardia? J. Cardiovasc. Electrophysiol. 19 (9) (2008) 977–978, https://doi.org/10.1111/j.1540-8167.2008.01179.x.

[8] B. Olshansky, R.M. Sullivan, Inappropriate sinus tachycardia, J. Am. Coll. Cardiol. 61 (8) (2013) 793–801, https://doi.org/10.1016/j.jacc.2012.07.074.

[9] R.J. Lee, J.M. Kalman, A.P. Fitzpatrick, L.M. Epstein, et al., Radiofrequency catheter modification of the sinus node for "inappropriate" sinus tachycardia, Circulation 92 (10) (1995) 2919–2928, https://doi.org/10.1161/01.CIR.92.10.2919.

[10] K.C. Man, B. Knight, H.F. Tse, F. Pelosi, et al., Radiofrequency catheter ablation of inappropriate sinus tachycardia guided by activation mapping, J. Am. Coll. Cardiol. 35 (2) (2000) 451–457, https://doi.org/10.1016/s0735-1097(99)00546-x.

[11] D.J. Callans, J.F. Ren, D. Schwartzman, C.D. Gottlieb, et al., Narrowing of the superior vena cava-right atrium junction during radiofrequency catheter ablation for inappropriate sinus tachycardia: analysis with intracardiac echocardiography, J. Am. Coll. Cardiol. 33 (6) (1999) 1667–1670, https://doi.org/10.1016/s0735-1097(99)00047-9.

[12] P.A. Low, P. Sandroni, M. Joyner, W.K. Shen, Postural tachycardia syndrome (POTS), J. Cardiovasc. Electrophysiol. 20 (3) (2009) 352–358, https://doi.org/10.1111/j.1540-8167.2008.01407.x.

[13] E.E. Benarroch, Postural tachycardia syndrome: a heterogeneous and multifactorial disorder, Mayo Clin. Proc. 87 (12) (2012) 1214–1225, https://doi.org/10.1016/j.mayocp.2012.08.013.

[14] Ch.U. Kumari, A.S.D. Murthy, B.L. Prasanna, M.P.P. Reddy, et al., An automated detection of heart arrhythmias using machine learning technique: SVM, Mater. Today (2020), https://doi.org/10.1016/j.matpr.2020.07.088.

[15] O. Yildirim, P. Plawiak, Ru-San Tan, U.R. Acharya, Arrhythmia detection using deep convolutional neural network with long duration ECG signals, Comput. Biol. Med. 102 (2018) 411–420, https://doi.org/10.1016/j.compbiomed.2018.09.009.

[16] T. Tabassum, M. Islam, An approach of cardiac disease prediction by analyzing ECG signal, 3rd International Conference on Electrical Engineering and Information Communication Technology (ICEEICT) (2016) 1–5, https://doi.org/10.1109/CEEICT.2016.7873093.

[17] M. Samuels, et al., Effectiveness and cost of recruiting healthy volunteers for clinical research studies using an electronic patient portal: a randomized study, Clin. Transl. Sci. 1 (6) (2017) 366–372.

[18] G.F. Fletcher, G. Balady, V.F. Froelicher, L.H. Hartley, W.L. Haskell, M.L. Pollock, Exercise standards: a statement for healthcare professionals from the American Heart Association, Circulation 91 (1995) 580–615.

[19] E.O. Nishime, C.R. Cole, E.H. Blackstone, F.J. Pashkow, M.S. Lauer, Heart rate recovery and treadmill exercise score as predictors of mortality in patients referred for exercise ECG, JAMA 284 (11) (2020) 1392–1398.

[20] J. Zheng, et al., A 12 lead electrocardiogram database for arrhythmia research covering more than 10,000 patients, Sci. Data 7 (2020) 48.

[21] P. Pławiak, Novel methodology of cardiac health recognition based on ECG signals and evolutionary-neural system, Expert Syst. Appl. 92 (2018) 334–349.

[22] P. Pławiak, Novel genetic ensembles of classifiers applied to myocardium dysfunction recognition based on ECG signals, Swarm Evol. Comput. 39 (2018) 192–208.

[23] T. Tuncer, S. Dogan, P. Pławiak, U.R. Acharya, Automated arrhythmia detection using novel hexadecimal local pattern and multilevel wavelet transform with ECG signals, Knowledge Based Syst. 186 (2019) 104923.

[24] C. Chen, Z. Hua, R. Zhang, G. Liu, W. Wen, Automated arrhythmia classification based on a combination network of CNN and LSTM, Biomed. Signal Process. Control 57 (2020) 101819.

[25] Z.I. Whinnett, S.M.A. Sohaib, D.W. Davies, Diagnosis and management of supraventricular tachycardia, BMJ 345 (2012) 7769.

[26] H.B. Braiek, F. Khomh, On testing machine learning programs, J. Syst. Softw. 164 (2020).

[27] V. Martínez, R. Alcaraz, J.J. Rieta, Study on the P-wave feature time course as early predictors of paroxysmal atrial fibrillation, Physiol. Meas. 33 (November) (2012) 1959–1974.

[28] P.G. Platonov, P-wave morphology: underlying mechanisms and clinical implications, Ann. Noninvasive Electrocardiol. 17 (July) (2012) 161–169.

[29] E.Z. Soliman, M. Cammarata, Y. Li, Explaining the inconsistent associations of PR interval with mortality: the role of P-duration contribution to the length of PR interval, Heart Rhythm 11 (January) (2014) 93–98.

[30] A.S. Manolis, K. Lazaridis, Focal atrial tachycardia ablation: highly successful with conventional mapping, J. Interv. Card. Electrophysiol. 55 (1) (2019) 35–46, https://doi.org/10.1007/s10840-018-0493-1.

[31] A.M. Zedda, F. Torri, L. Bertagnolli, A. Arya, Changing P-wave morphology: what is the mechanism? J. Electrocardiol. 50 (4) (2017) 510–512, https://doi.org/10.1016/j.jelectrocard.2017.02.005.

[32] J. Tanabe, S. Fujita, N. Watanabe, K. Tanabe, A case of prolonged atrial pacing latency, EHJ-Case Rep. 4 (4) (2020) 1–2, https://doi.org/10.1093/ehjcr/ytaa215.

[33] G.M. Morris, L. Segan, G. Wong, G. Wynn, T. Watts, et al., Atrial tachycardia arising from the crista terminalis, detailed electrophysiological features, and long-term ablation outcomes, J. Am. Coll. Cardiol. EP. 5 (4) (2019) 448–458, https://doi.org/10.1016/j.jacep.2019.01.014.

[34] J.Y. Li, X.W. Lv, G.Q. Zhong, H.H. Ke, Micro-reentry right atrial tachycardia originating from fossa ovalis: a case report of high-density mapping by PentaRay catheter, EHJ- Case Rep. 3 (3) (2019), https://doi.org/10.1093/ehjcr/ytz141.

[35] K. Hayashi, S. Mathew, C.H. Heeger, T. Maurer, et al., Pace mapping for the identification of focal atrial tachycardia origin, Circ. Arrhythm. Electrophysiol. 9 (7) (2016), https://doi.org/10.1161/CIRCEP.116.003930.

[36] M.R. Sonsoz, A.K. Bilge, A. Elitok, Left atrial appendage: the uncommon origin of focal atrial tachycardia in a pregnant woman, Anatol. J. Cardiol. 22 (6) (2019) 5013–5014, https://doi.org/10.14744/AnatolJCardiol.2019.17748.

[37] L.L. Eckhardt, M.H. Hamdan, Inappropriate sinus tachycardia, in: Marek Malik (Ed.), Sex and Cardiac Electrophysiology, 1, 2020, pp. 453–462.

[38] J. Sivaraman, G. Uma, S. Venkatesan, M. Umapathy, V.E. Dhandapani, Normal limits of ECG measurements related to atrial activity using a modified limb lead system, Anatol. J. Cardiol. 15 (1) (2015) 2–6, https://doi.org/10.5152/akd.2014.5155.

[39] J. Sivaraman, G. Uma, S. Venkatesan, M. Umapathy, K.N. Keshav, A study on atrial Ta wave morphology in healthy subjects: an approach using P wave signal-averaging method, J. Med. Imaging Health Inf. 4 (5) (2014) 675–680, https://doi.org/10.1166/jmihi.2014.1306.

[40] J. Sivaraman, S. Venkatesan, R. Periyasamy, J. Joseph, R.M. Shanmugan, Modified limb lead ECG system effects on electrocardiographic wave amplitudes and frontal plane axis in sinus rhythm subjects, Anatol. J. Cardiol. 17 (1) (2017) 46–54, https://doi.org/10.14744/AnatolJCardiol.2016.6843.

[41] R. John, J. Sivaraman, Effects of Sinus Rhythm on Atrial ECG Components Using a Modified Limb Lead System, ISPCC, 2017, pp. 527–530, https://doi.org/10.1109/ISPCC.2017.8269735.

[42] S. Karimulla, J. Sivaraman, in: P.K. Mallick, P. Meher, A. Majumder, S.K. Das (Eds.), The Role and Significance of Atrial ECG Components in Standard and Modified Lead Systems, ESIC, 2020, p. 686, https://doi.org/10.1007/978-981-15-7031-5_33.

[43] A. Jyothsana, J. Sivaraman, in: P.K. Mallick, P. Meher, A. Majumder, S.K. Das (Eds.), A Study on Stability Analysis of QT Interval Dynamics of ECG Using ARMAX Model, ESIC, 2020, p. 686, https://doi.org/10.1007/978-981-15-7031-5_29.

[44] A. Jyothsana, B. Arya, J. Sivaraman, Stability analysis on the effects of heart rate variability and premature activation of atrial ECG dynamics using ARMAX model, Phys. Eng. Sci. Med. 9 (2020), https://doi.org/10.1007/s13246-020-00940-w.

[45] K. Nagashima, Y. Wakamatsu, S. Kurokawa, N. Otsuka, S. Yagyu, Y. Okumara, Minimally preexcited tachycardia: what is the mechanism? Heart Rhythm –Case Rep. 6 (10) (2020) 805–807, https://doi.org/10.1016/j.hrcr.2020.07.001.

[46] M.E. Field, et al., P-wave amplitude and PR changes in patients with inappropriate sinus tachycardia: findings supportive of a central mechanism, J. Am. Heart Assoc. 7 (9) (2018), https://doi.org/10.1161/jaha.118.008528.

[47] A. Madaffari, et al., Ablation of typical atrial flutter guided by the paced PR interval on the surface electrocardiogram: a proof of concept study, Europace 21 (11) (2019) 1750–1754, https://doi.org/10.1093/europace/euz208.
[48] J. Sivaraman, G. Uma, P. Langley, M. Umapathy, S. Venkatesan, G. Palanikumar, A study on stability analysis of atrial repolarization variability using ARX model in sinus rhythm and atrial tachycardia ECGs, Comput Meth Prog Bio. 137 (2016) 341–351, https://doi.org/10.1016/j.cmpb.2016.10.005.
[49] S. Cabrera, E. Valles, B. Benito, O. Alcalde, J. Jimenez, R. Fan, J. Marti-Almor, Simple predictors for new-onset atrial fibrillation, Int. J. Cardiol. 221 (2016) 515–520, https://doi.org/10.1016/j.ijcard.2016.07.077.
[50] B.B. Pavri, J. Kloo, D. Farzad, J.M. Riley, Behavior of the PR interval with increasing heart rate in patients with Covid-19, Heart Rhythm 17 (9) (2020) 1434–1438, https://doi.org/10.1016/j.hrthm.2020.06.009.
[51] B. Banavalikar, et al., Clinical and electrophysiological correlates of incessant ivabradine-sensitive atrial tachycardia, Circ. Arrhythm. Electrophysiol. 12 (8) (2019), https://doi.org/10.1161/circep.119.007387.
[52] K.T. Kang, et al., Current management of focal atrial tachycardia in children: a multicenter experience, Circ. Arrhythm. Electrophysiol. 7 (4) (2014) 664–670, https://doi.org/10.1161/CIRCEP.113.001423.
[53] B. Dhananjay, J. Sivaraman, The role of heart rate variability in atrial ECG components of normal sinus rhythm and sinus tachycardia subjects, in: S. Satapathy, V. Bhateja, B. Janakiramaiah, Y.W. Chen (Eds.), Intelligent System Design. Advances in Intelligent Systems and Computing, 1171, 2021, pp. 637–644, https://doi.org/10.1007/978-981-15-5400-1_61.
[54] F.A. Elhaj, N. Salim, A.R. Harris, T.T. Swee, T. Ahmed, Arrhythmia recognition and classification using combined linear and non-linear features of ECG signals, Comput. Meth Prog. Bio. 127 (2016) 52–63, https://doi.org/10.1016/j.cmpb.2015.12.024.
[55] C.K. Jha, M.H. Kolekar, Cardiac arrhythmia classification using tunable Q – wavelet transform based features and support vector machine classifier, Biomed. Signal Process. Control 59 (2020), https://doi.org/10.1016/j.bspc.2020.101875.
[56] V. Mondejar-Guerra, J. Novo, J. Rouco, M.G. Penedo, M. Ortega, Heartbeat classification fusing temporal and morphological information of ECGs via ensemble of classifiers, Biomed. Signal Process. Control 47 (2019), https://doi.org/10.1016/j.bspc.2018.08.007.
[57] S. Chen, W. Hua, Z. Li, J. Li, X. Gao, Heartbeat classification using projected and dynamic features of ECG signal, Biomed. Signal Process. Control 31 (2017), https://doi.org/10.1016/j.bspc.2016.07.010.
[58] U.R. Acharya, J.E.W. Koh, R.J. Martis, V.K. Sudarshan, Application of higher-order spectra for the characterization of Coronary artery disease using electrocardiogram signals, Biomed. Signal Process. Control 31 (2017) 31–43, https://doi.org/10.1016/j.bspc.2016.07.003.
[59] Q. Li, R. Cadathur, D.C. Gari, Ventricular fibrillation and tachycardia classification using a machine learning approach, IEEE Trans. Biomed. Eng. 61 (6) (2013) 1607–1613, https://doi.org/10.1109/TBME.2013.2275000.
[60] S.M. Abubakar, W. Saadeh, M.A.B. Altaf, A wearable long-term single-lead ECG processor for early detection of cardiac arrhythmia, 2018 Design, Automation & Test in Europe Conference & Exhibition (DATE) (2018) 961–966, https://doi.org/10.23919/DATE.2018.8342148.
[61] S.M. Abubakar, M.R. Khan, W. Saadeh, M.A.B. Altaf, A wearable auto-patient adaptive ECG processor for shockable cardiac arrhythmia, 2018 IEEE Asian Solid-State Circuits Conference (A-SSCC) (2018) 267–268, https://doi.org/10.1109/ASSCC.2018.8579263.
[62] D. Jeon, et al., An implantable 64nW ECG-monitoring mixed-signal SoC for arrhythmia diagnosis, IEEE ISSCC Dig. Tech. Papers. (2014) 416–417.
[63] M.A. Sohail, Z. Taufique, S.M. Abubakar, W. Saadeh, M.A.B. Altaf, An ecg processor for the detection of eight cardiac arrhythmias with minimum false alarms, 2019 IEEE Biomedical Circuits and Systems Conference (BioCAS) (2019) 1–4, https://doi.org/10.1109/BIOCAS.2019.8919053.